M. Klost, C. Brzeski, S. Drusch

Effect of protein aggregation on rheological properties of pea protein gels

Klost, M., Brzeski, C., & Drusch, S. (2020). Effect of protein aggregation on rheological properties of pea protein gels. Food Hydrocolloids, 108, 106036. https://doi.org/10.1016/j.foodhyd.2020.106036

Effect of protein aggregation on rheological properties of pea protein gels

M. Klost[1, 2], C. Brzeski[1] and S. Drusch[1, 2]

[1] Technische Universität Berlin, Faculty III Process Sciences, Institute of Food technology and Food Chemistry, Department of Food Technology and Food Material Science, Straße des 17. Juni 135, 10623 Berlin, Germany

[2] NutriAct – Competence Cluster Nutrition Research Berlin-Potsdam

* Correspondence: martina.klost@tu-berlin.de

ABSTRACT

Yoghurt style gels are a promising way to increase the consumption of plant derived proteins. However, reaching texture properties similar to those commonly known from milk yoghurts while incorporating large amounts of plant-derived proteins, is a challenge that needs to be addressed to meet consumers expectations. Therefore, this study aims to investigate the influence of pH conditions (pH 6.0 to pH 8.0) during pre-treatment on the rheological properties of fermentation induced pea protein gels with a protein content of 10%. Results showed a strong correlation between the pH value during pre-treatment and the protein solubility after pH readjustment to pH 8. Solubility was highest if pea protein was pre-treated at pH 8.0 and lowest if it was pre-treated at pH 6.0. Since only soluble aggregates are believed to participate in network formation, networks formed by pea protein pre-treated at pH 6 were coarser, than those formed by pea protein pre-treated at pH 8 owing to a lower degree of crosslinking caused by less available protein. Coarser networks and higher proportions of insoluble particles increased loss of water and lowered the storage modulus G' as well as the ability of the networks to recover after intense shearing. In particular pre-treatment at pH values below 7.0 led to gels with storage moduli of the same magnitude as those measured in commercial milk derived yoghurts. Adjusting the pH value during pre-treatment of pea protein can therefore be considered a promising approach for the customisation of texture properties while maintaining a constantly high protein content.

1. INTRODUCTION

In the light of increasing life expectancy, it is inevitable to address the issue of age related non-communicable diseases in a preventive manner (WHO, 2013). One approach is to increase consumer awareness for a healthy lifestyle and a balanced nutrition and to provide a range of corresponding foods. In this context, plant derived proteins have been proposed to contribute to the prevention of chronic degenerative diseases (Krajcovicova-Kudlackova, Babinska, & Valachovicova, 2005). As a consequence, an adequate intake through consumption of plant -based foods needs to be achieved. Plant protein-enriched beverages and emulsion products cannot deliver the required amounts of plant derived protein for this purpose. In contrast, gels are dispersed systems more suitable for the incorporation of relevant amounts of plant derived protein. E. g. yoghurt has a high consumer acceptance when it comes

to protein-rich foods (Banovic et al., 2018), and yoghurt type products from plant derived proteins allow for the incorporation of up to at least 10% plant derived protein (Klost & Drusch, 2019; Klost, Giménez-Ribes, & Drusch, 2020).

Plant-derived proteins (such as pea and soy) consist of hexameric 11S and trimeric 7S globular protein fractions. The general process of acid induced gelation has been extensively described by a variety of authors and for proteins from various plants. It starts with a heating step during which the protein undergoes heat induced structural rearrangements that lead to the formation of aggregates. When electrostatic repulsion is lowered during acidification, soluble aggregates form network structures by hydrophobic interactions e. g. (Ringgenberg, Alexander, & Corredig, 2013). However, during heat treatment – apart from the soluble aggregates required for gelation – insoluble aggregates may form. Whether soluble or insoluble aggregates are formed depends on the sensitivity of the different protein fractions to environmental factors like ionic strength, temperature and pH conditions (Yamagishi, Miyakawa, Noda, & Yamauchi, 1983). In this context, changes in pH conditions or ionic strength may decrease the electrostatic repulsion between two particles (Cano-Sarmiento et al., 2018) and consequently promote short range particle interactions (Klemmer, Waldner, Stone, Low, & Nickerson, 2012). Generally, differences in sensitivity towards environmental factors can lead to a variety of aggregates that are formed between different protein fractions and/or different protein fraction subunits via disulphide or non-covalent bonds. Due to lack of detailed studies on the aggregation behaviour of pea protein and vast similarities between pea and soy proteins we refer to literature on soy protein as an indicator for pea protein's aggregation behaviour. Generally speaking, various 7S and 11S fractions can form aggregates with other 7S or 11S fractions via various types of interactions. A summary of soy protein fractions and types of interactions involved in those soluble and insoluble aggregates is given in table 1.

Table 1 types of aggregates formed upon heating of mixtures of soy 11S and 7S: types of interactions involved in aggregate formation and composition of aggregates (corresponding pea proteins are: 11S → Legumin, 7Sαα' → Convicilin, 7Sβ → Vicilin)

	subunits involved	interactions	reference
soluble	7S αα'	disulphide bond	(Yamagishi et al., 1983)
	7S αα' and 11S acidic	disulphide bond	(Yamagishi et al., 1983)
	7S β and 11S basic	disulphide bond	(Damodaran & Kinsella, 1982; German, Damodaran, & Kinsella, 1982)
	7S αα' and 7S β	no disulphide bond	(Yamagishi et al., 1983)
	7S β	no disulphide bond	(Yamagishi et al., 1983)
	7S β and 11S basic	no disulphide bond	(Petruccelli & Añón, 1995)
insoluble	11S acidic and basic	disulphide bond	(Yamagishi et al., 1983)
	7S αα' and 11S acidic+basic	disulphide bond	(Yamagishi et al., 1983)
	7S β	no disulphide bond	(Yamagishi et al., 1983)
	11S basic	no disulphide bond	e.g. (German et al., 1982)

Different ratios of soluble to insoluble aggregates may influence a protein's ability to form fermentation induced gels. While soluble aggregates are a prerequisite for the formation of fermentation induced gels e. g. (Ringgenberg et al., 2013) insoluble aggregates may act as inactive fillers and weaken an emerging gel matrix (Britten & Giroux, 2001). Weakened gel matrices should in turn be reflected in rheological and texture parameters. In two previous studies (Klost & Drusch, 2019; Klost et al., 2020) with different objectives – and therefore different environmental parameters such as pH, homogenisation pressure, heating temperature and heating time during protein pre-treatment prior to fermentation – we found relevant inter-study differences in rheological moduli G' and G''. While for the first study no specific pre-treatment – apart from heating – was performed (Klost & Drusch, 2019), we additionally applied enzymatic hydrolysis as a pre-treatment before fermentation in the second study (Klost et al., 2020). In preliminary experiments from this study we tested different pH values (pH 7.0, 7.5 and 8.0) during hydrolysis for one of the applied enzymes (Protamex®) to determine its pH optimum (unpublished data). Interestingly, we found significant differences between the storage moduli G' at the end of fermentation but no differences in the molecular weight distribution of the corresponding hydrolysates (supplementary fig S1). G' decreased from 5052 ± 172 Pa (hydrolysis at pH 8.0) to 1487 ± 180 Pa (hydrolysis at pH 7.0). Putting these values in line with the results from the first study (complex shear modulus $|G^*|$ = 452 ± 27 Pa (corresponding to storage modulus G' = 446 ± 26 Pa)) where heating was conducted at pH ~6.5 we suspect the influence of pH value during heat pre-treatment to be the most important parameter for these inter-study differences. However, this presumption needs to be confirmed in a systematic investigation.

Therefore, the focus of this study is to investigate the application of pH variation during pre-treatment of pea protein to specifically customise the rheological properties of subsequently produced yoghurt alternatives. To this regard, we propose the following mechanism by which the pH value during pre-treatment (heating and homogenising) influences the aggregation behaviour of pea protein: at a pH that leads to reduced electrostatic repulsion close-range interactions lead to an increase in insoluble aggregates. A higher proportion of insoluble aggregates will weaken the gel structure and will result in less stable gels. With this in mind it should be possible to customise the rheological properties of fermentation induced pea protein gels by targeted manipulation of environmental parameters during a pre-treatment step prior to fermentation while maintaining the protein content constant at 10%. Moreover, beyond the development of yoghurt alternatives, customising the texture of fermentation induced pea-protein gels may lead to a variety of new products such as spreads, cream fillings for bakery and confectionary products, etc. in the future.

2. MATERIALS AND METHODS

Fig 1 gives a general overview over the experimental setup. In a first set of experiments the difference in intrinsic fluorescence before and after heating, the ζ-potential and the protein solubility, of the untreated protein were analysed in dependence of the pH value to gain a deeper understanding of the unfolding behaviour during heating, the electrostatic properties and the formation of insoluble aggregates respectively. Slurries with a protein content of 10% were prepared from this raw material. In subsequent steps the pH of the slurries was adjusted according to the experimental setup, the slurries were heated and homogenised followed by pH readjustment to pH 8. Afterwards these pre-treated slurries were either lyophilised for molecular weight analysis and further protein solubility tests, or fermented for subsequent rheological, microscopic and loss of water characterisation.

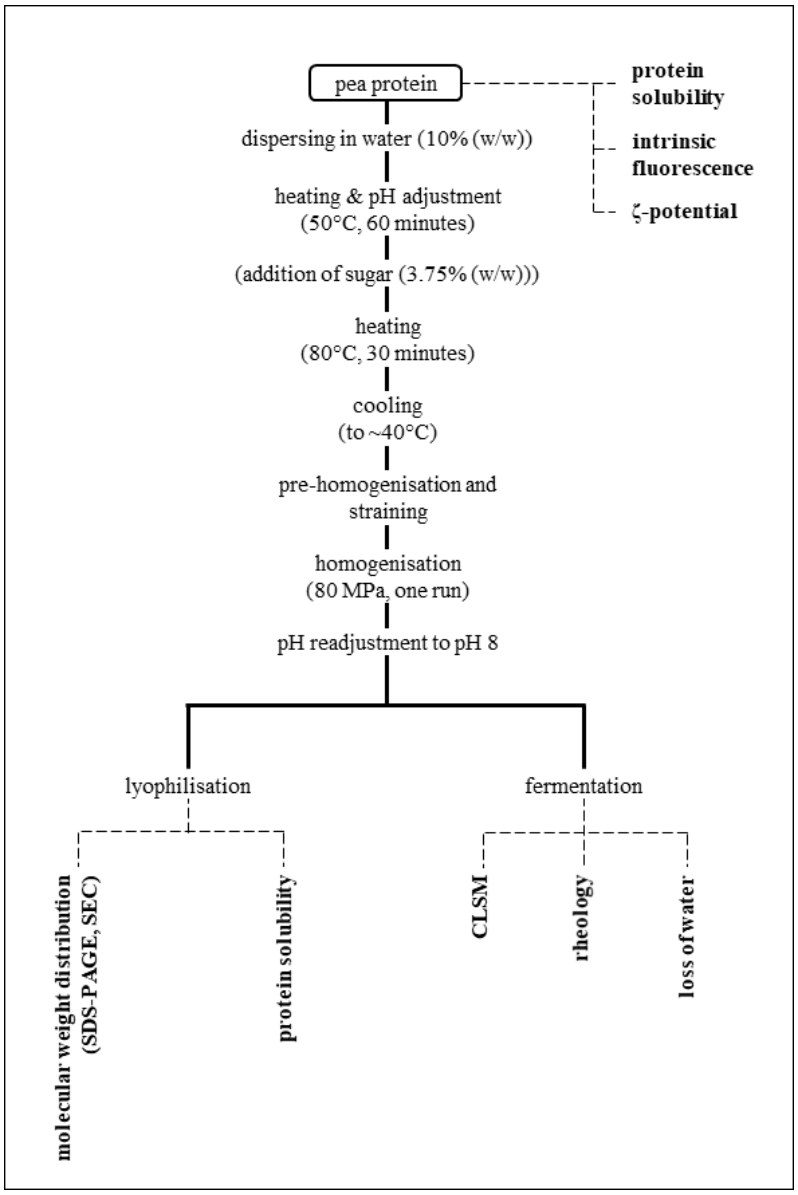

Fig 1 flow chart of experimental setup

Materials

Pea protein concentrate (LOT-Nr.: 16041801) with a protein content of 78% was obtained from IGV (Institut für Getreideverarbeitung) GmbH, Nuthetal, Germany. The lactic acid culture (YoFlex®; *S. thermophilus* and *L. bulgaricus*) was kindly provided by Chr. Hansen, Hoersholm, Denmark. Gels and buffer-solutions for SDS-PAGE analysis were purchased from BioRad Laboratories GmbH (München, Germany). All other chemicals were of analytical grade and purchased from Merck and Sigma Aldrich (Darmstadt, Germany) and Carl Roth GmbH + Co.KG (Karlsruhe, Germany).

ζ-potential measurement of untreated pea protein

ζ-potential measurements were conducted to estimate the electrostatic repulsive properties of the untreated protein in dependence of the pH-value. Measurements were carried out in triplicate in protein solutions containing 0.3% (w/w) of the untreated protein prepared in 0.01 M phosphate buffer at pH 6.0, 6.5, 7.0, 7.5, 8.0 (Zetasizer Nano-ZS, Malvern Instruments GmbH, Herrenberg, Germany).

Determination of intrinsic fluorescence of untreated pea protein

Intrinsic fluorescence measurements were carried out in order to determine differences in the unfolding behaviour of pea protein, when heated at different pH values. Protein solutions of 0.05% (w/w) protein in 0.01 M phosphate buffer were prepared at pH 6.0, 6.5, 7.0, 7.5 and 8.0. Samples were measured in a Cary Eclipse Fluorescence Spectrophotometer (Agilent Technologies, Victoria, Australia) at an excitation wavelength of 290 nm and the emission wavelength was scanned between 300 and 400 nm. Emission wavelengths were scanned before heating, followed by subsequent heating to 50 °C, holding for 60 minutes, further heating to 80 °C, holding for 30 minutes and another scan of the emission wavelength. All samples were prepared in triplicate. For evaluation the wavelengths at maximum emission before and after heating were determined and the red shift during heating was calculated as the difference between the two values.

Solubility of pea protein

Protein solubility was measured before and after the pre-treatment process and before fermentation. More specific, the solubility of the raw material was measured at pH 6 to 8 with steps of 0.5, the solubility of pre-treated and freeze-dried samples was measured at the pH value during pre-treatment as well as at pH 8 representing the pH at the start of fermentation. To this purpose, suspensions with a protein content of 5% were prepared and the pH values were readjusted to the required value with 0.1 M/1 M NaOH or 0.1 M/1 M HCl if necessary. Suspensions were then left to stir for 60 minutes. An aliquot of the suspensions was used to determine the total protein content and another aliquot was centrifuged at 10000xg for 15 minutes for the determination of the soluble protein fraction. Protein contents were determined with a Dumatherm® (C. Gerhardt GmbH&Co. KG, Königswinter, Germany) at an oxygen flow rate of 100 mL/min and 0.8 mg oxygen/mg sample. Protein solubility was then calculated as

$$\text{protein solubility} = \frac{c_{\text{soluble protein}}}{c_{\text{total protein}}} \cdot 100\% \quad (1)$$

Pea protein pre-treatment, lyophilisation and fermentation

A protein slurry (10% protein (w/w)) was heated to 50 °C under constant stirring and the pH value was adjusted to 6.0, 6.5, 7.0, 7.5 or 8.0 respectively with 1 M NaOH and/or 1 M HCl. After a holding time of 60 minutes 3.75% (w/w) sugar was added to slurries for fermentation, the temperature was increased to 80 °C and the sample was held for further 30 minutes followed by cooling to approximately 40 °C in an ice bath. Samples for lyophilisation were prepared without the addition of sugar. The cooled slurries were pre-homogenised (Ultraturrax T25 basic, IKA, Germany, 30 s, 17500 rpm), strained through a sieve and high pressure homogenised (Panda Plus, Niro Soavi, Germany, 80 MPa, one run). To samples for fermentation, starter culture (YC-X11 Yo-Flex®, Chr. Hansen, Hoersholm, Denmark) was added subsequently and the samples were filled into centrifuge tubes for loss of water experiments, beaker for confocal laser scan microscopy (CLSM) and disposable rheology cups (Cat No 3716, Anton Paar, Graz, Austria) for rheological tests. Samples were then fermented in a water-bath at 43 °C for 18 h. After fermentation, the samples were stored at 4 °C for 24 hours before further investigation. Samples for lyophilisation were frozen in an ethanol bath after homogenisation followed by lyophilisation. All samples were prepared in triplicate for fermentation and lyophilisation. Additionally, one repetition of each sample was prepared for CLSM experiments.

Molecular weight distribution of pre-treated and lyophilised pea protein via SDS-PAGE and size exclusion chromatography

SDS-PAGE on 12% Criterion™ TGX™ Gels (26 wells) (BioRad Laboratories GmbH, München, Germany) was used to characterise the molecular weight profiles of pre-treated and lyophilised samples. Experiments were conducted according to the BioRad Bulletin #4110001 under reducing and non-reducing conditions with Biorad 10xTris/Glycine/SDS (Cat# 161-0732) as running buffer. Sample concentration was 0.1% in sample buffer (Biorad 2xLaemmli sample buffer, Cat# 161-0737 with or without addition of dithiothreitol) and 10 µL of the samples were applied to the gels alongside a molecular weight marker (PageRuler™ Prestained Protein Ladder, Cat# 26616, ThermoScientific). Evaluation of the gels was carried out via photography of the gels followed by band identification via estimation of their position in relation to the marker in combination with reference values from literature and transformation to peaks for presentation (open source software ImageJ 1.52d (Schneider, Rasband, & Eliceiri, 2012)). Transformation to peaks was done as mean of three gel lanes.

Size exclusion chromatography (SEC) of lyophilised samples (0.1% (w/w) in 0.1 M phosphate buffer, pH 8) was performed in triplicate on a Superdex 200 Increase 10/300 GL (GE healthcare GmbH, Solingen, Germany) column with 0.1 M phosphate buffer as eluent (HPLC ÄKTAbasicTM 10 system, Amersham Biosciences, Uppsala, Sweden). Detection took place via an UV detector at 280 nm. Qualification of peaks was not possible, but determination of the calibration area was performed by using the highest and lowest calibration points from previous experiments.

Confocal laser scan microscopy (CLSM) of fermentation induced pea protein gels

For CLSM, 20 µl rhodamine B solution (0.2% (w/w) in distilled water) per gram sample were added to the protein suspension before fermentation. CLSM was performed on one set of fermented samples. The microscope was a Leica SP8 (Leica Microsystems GmbH, Wetzlar, Germany) with a HC PL APO CS2 63x/1.20 water objective (pinhole at airy unit 1 AU (111.5 µm)). Image resolution was 512x512 pixels. For GFP detection a 3% laser (552 nm) intensity was coupled with emission detection of 580 nm at a gain of 357. The number of required z-stacks was determined using the system optimised calculation of z-stacks.

Loss of water

The fermented samples in the centrifuge tubes were centrifuged (500 g, 20 °C, 10 minutes, Avanti J-E, Beckman Coulter GmbH, Krefeld, Germany) in a method adapted from (Guzmán-González, Morais, Ramos, & Amigo, 1999). Subsequently the supernatant was discarded and the remaining sample was weight. Loss of water was calculated as:

$$\text{loss of water} = \frac{\text{mass}_{\text{total}}\text{-mass}_{\text{pellet}}}{\text{mass}_{\text{total}}} \cdot 100\% \qquad (2)$$

Rheology

Determination of all rheological properties was carried out in triplicate on an MCR 502 (Anton Paar, Austria, concentric cylinder system CC 27 (measuring bob radius = 13.33 mm, measuring cup radius = 14.46 mm, gap length = 40 mm)). For time-sweeps additional rheometers were used (Physica UDS and MCR 301, Anton Paar, Austria, concentric cylinder system Z 3 DIN (measuring bob radius = 12.5 mm, measuring cup radius = 13.56 mm, gap length = 37.5 mm) and CC 27 (measuring bob radius = 13.33 mm, measuring cup radius = 14.46 mm, gap length = 40 mm) respectively). Special care was taken, that replications of each sample were performed on at least two different rheometers. Time sweeps were carried out during fermentation at 43 °C for 18 hours (f = 1 Hz, γ = 0.1%) in order to track the structuring process. G' and tan δ were chosen as parameters for evaluation. Thixotropy tests were performed according to DIN SPEC 91143-2, 2012: samples were oscillated (f = 1 Hz, γ = 0.1%) for 120 s followed by shearing for 120 s at $\dot{\gamma} = 200\ s^{-1}$ and oscillation for another 300 seconds. From these experiments recovery of structure was calculated as:

$$\text{recovery} = \frac{G'_{\text{End}}}{G'_{\text{Start}}} \cdot 100\%. \qquad (3)$$

Frequency sweeps were conducted at γ = 0.1% and frequencies ranging from 10 Hz to 0,01 Hz. For evaluation the slopes dlogG' / dlogω from the double logarithmic plots were determined and compared.

For the characterisation of non-linear deformation behaviour, amplitude-sweeps were performed at f = 1 Hz and strain amplitude γ_0 between 0.01% and 1000%. First of all, the end of the linear viscoelastic regime was determined as the point, where G' varies more than 5% from the original value. Evaluation of the non-linear deformation was carried out via Lissajous plots, stress decomposition and calculation of the stiffening ratio (S-factor) and dissipation ratio φ. In this context, information about both inter- and intracycle behaviour can be derived from Lissajous plots and the interpretation of the elastic stress curves can contribute to understanding changes within the network structure by application of a model that links rupture of colloidal gels to the bond number between individual particles in the gel network e.g. (Hsiao, Newman, Glotzer, & Solomon, 2012; Park & Ahn, 2013; Park et al., 2015) or the description of microcracks that occur prior to the complete rupture of gels (Faber, Van Breemen, & McKinley, 2017). Consequently, perfectly elastic behaviour – represented by a straight line in the intracycle strain γ-elastic stress τ' diagram – is related to a rigid cluster structure with high bond numbers (i.e. 4 to 6) in the gels (Park et al., 2015). At intercycle strain amplitude γ_0 above the linear viscoelastic regime, shear and strain amplitude begin to interfere with the network structures. Depending on the applied model, this may be reflected in the decrease of bonding numbers e.g. (Hsiao et al., 2012; Park & Ahn, 2013; Park et al., 2015) or the occurrence of microcracks (Faber et al., 2017). Both would reduce the size and volume fraction of rigid clusters which in turn leads to a reduction in the load bearing network that would be capable of supporting elastic stress (Hsiao et al., 2012). If such behaviour occurs, it is reflected in the onset of deviation of the curves from a straight line. This deviation often leads to an inversed sigmoidal shape. This shape can be interpreted as follows: the decline of the slope at small intracycle strain γ indicates a decrease in the ability to support elastic stress owing to the reduced size and volume fraction of rigid clusters (Park et al., 2015) and therefore relates to overall intercycle strain softening with increasing intercycle strain amplitude γ_0. The increase of the slope at higher intracycle strain γ can be related to the stretching of remaining rigid clusters which in turn causes strong intracycle elasticity (Park et al., 2015) and indicates intracycle stiffening. The calculation of S-factors reflects this intracycle behaviour onto the entire range of intercycle strain amplitudes γ_0. S-factors were calculated according to (Ewoldt, Hosoi, & McKinley, 2008):

$$S \equiv \frac{G'_L - G'_M}{G'_L} \tag{4}$$

where G'_L is the large strain modulus (secant line of elastic Lissajous plot) and G'_M is the minimum strain modulus (slope of elastic Lissajous plots at zero). In this context an S-factor $S > 0$ indicates intracycle strain stiffening, whereas $S < 0$ refers to intracycle strain softening (Ewoldt et al., 2008). However, when evaluating S-factors the special case of pseudoplastic and elastoviscoplastic materials needs to be considered. While in truly strain stiffening systems the overall stress will increase towards higher intracycle strains γ (elastic Lissajous plot) as shown by Park et al in their fig 11 (Park, Ahn, & Lee, 2015) and by Ewoldt et al in their fig 10 (Ewoldt, Winter, Maxey, & McKinley, 2010) and the S-factor may become $S > 1$, in pseudoplastic and elastoviscoplastic materials the overall stress may

approach a perfectly rectangular shape in elastic Lissajous plots (Ewoldt et al., 2010) and the S-factor will trend towards a maximum value of one. Especially in the latter case the elastic stress curve will be horizontal at low intracycle strain γ and its slope may increase towards higher intracycle strain γ. This leads to the S-factors trending towards one – and therefore $S > 0$ – despite a strain softening overall rheology (Mermet-Guyennet et al., 2015). This effect is owing to the mathematical definitions of the S-factor (Ewoldt et al., 2010). More specifically, in this case the tangent modulus at minimum intracycle strain γ (G_M) approaches zero and therefore equation 2 reduces to

$$\text{S-factor} = \frac{G_L}{G_L} = 1 \text{ (Ewoldt et al., 2010)} \quad . \tag{4a}$$

In order to distinguish between true intracycle strain stiffening and a shift from predominantly elastic to mainly plastic behaviour it is therefore important, to consider the S-factor in combination with the dissipation ratio φ (Ewoldt et al., 2010)

$$\varphi = \frac{E_D}{E_{D,pp}} = \frac{\pi \gamma_0 G''}{4\tau_{max}} \tag{5}$$

where E_D is the dissipated energy per cycle and corresponds to the area enclosed by the elastic Lissaous plot, $E_{D,pp}$ is the dissipated energy in the corresponding perfect plastic system, γ_0 is the intercycle strain amplitude, G'' is the loss modulus at that stain amplitude and τ_{max} is the maximum shear stress in the considered oscillatory cycle. In this context the dissipation ratio φ relates the dissipated energy in the sample to the dissipated energy in a corresponding perfectly plastic material and consequently allows to categorise rheological behaviour into elastic ($\varphi \rightarrow 0$) or plastic ($\varphi \rightarrow 1$) behaviour with a known critical value ($\varphi = \pi/4$) for Newtonian behaviour (Ewoldt et al., 2010).

All data was obtained and – except for the dissipation ratio φ – automatically calculated by RheoCompass™ Software (Anton Paar, Austria)

3. RESULTS & DISCUSSION

Protein characterisation

Electrostatic interactions and unfolding properties of untreated pea protein

The ζ-potential reflects electrostatic interactions between individual protein molecules and depends on the pH value of the surrounding medium. Results show, that the absolute value of the ζ-potential significantly decreased from |20.4| ± 0.5 mV to |11.7| ± 1.0 mV with decreasing pH values during pre-treatment (table 2) indicating lower electrostatic repulsion at lower pH values. However, it is generally accepted, that ζ-potentials above |30| mV are a prerequisite for full electrostatic stabilisation. As a general rule, stability of hydrocolloid stabilised oil-droplets with ζ-potentials below |15| mV cannot exclusively be explained by double-layer repulsion (Dickinson, 2009) and (Piorkowski & McClements,

2014) recommend ζ-potentials above |20| mV for long-term stability of electrostatically stabilised beverage emulsions.

Table 2 ζ-potential and protein solubility before heating, protein solubility of heated, homogenised and lyophilised protein at the original pH value and at pH 8 simulating the beginning of fermentation and red shift during heating of the protein.

sample	ζ-potential before heating [mV]	Protein solubility unheated samples [%]	Protein solubility heated samples [%]	Protein solubility heated samples at pH 8 [%]	red shift during heating [nm]
pH 6.0	$-11.7^{a} \pm 1.0$	$20.8^{a,1} \pm 0.4$	$17.5^{a,2} \pm 0.9$	$37.6^{a,3} \pm 1.1$	$10.0^{(\blacklozenge)}$
pH 6.5	$-14.2^{b} \pm 0.6$	$26.0^{b,1} \pm 1.5$	$21.1^{a,b,2} \pm 0.3$	$40.0^{a,b,3} \pm 2.1$	$7.7^{a} \pm 4.0$
pH 7.0	$-17.1^{c} \pm 0.8$	$35.2^{c,1} \pm 1.9$	$27.4^{b,2} \pm 1.4$	$44.7^{a,b,3} \pm 3.1$	$8.3^{a} \pm 1.2$
pH 7.5	$-19.9^{d} \pm 0.8$	$63.9^{d,1} \pm 0.1$	$40.3^{c,2} \pm 3.4$	$47.1^{b,2} \pm 3.2$	$11.0^{a} \pm 2.0$
pH 8.0	$-20.4^{d} \pm 0.5$	$68.8^{e,1} \pm 1.2$	$57.2^{d,2} \pm 4.0$	$57.2^{c,2} \pm 4.0$	$7.0^{a} \pm 3.6$

Different letters represent significant differences (α=0.05) within columns, different superscript numbers represent significant differences (α=0.05) within rows as derived from ANOVA followed by Tukey post-Hoc test.

$^{(\blacklozenge)}$ value calculated from double determination due to equipment failure. Data point was excluded from ANOVA and post-Hoc test.

We therefore need to assume, that electrostatic stabilisation is insufficient to prevent flocculation at pH 6.0 and 6.5 and is inadequate to fully stabilise a protein dispersion at pH 7.0 and 7.5. In turn we can assume, that the chosen pH-range is suitable to produce samples with differently pronounced electrostatic repulsion, which may in turn lead to differences in aggregation. While the degree of electrostatic repulsion determines how close individual particles may get to each other, the aggregation itself may take place via further non-covalent interactions and via disulphide-bonds. The ability to form these types of interactions and bonds in turn strongly depends on the accessibility of relevant protein side chains and therefore on the protein unfolding. Protein unfolding can be determined via intrinsic fluorescence measurements. Generally, a red shift i.e. an increase in the wavelength at emission maximum represents the unfolding of a protein as indicated by the decrease in the interactions of tryptophan residues with quenching groups and thus an increase in its exposure to the solvent (Cairoli, Iametti, & Bonomi, 1994). In our study the red shift by 7 to 11 nm upon heating of protein solutions from 20 °C to 80 °C (table 2) was not significantly dependent on the pH value during pre-treatment. We therefore propose similar unfolding kinetics during heating in all samples. Consequently, the electrostatic repulsion – or lack thereof – must be the main influence factor on aggregation behaviour.

Protein solubility of untreated, pre-treated and pH readjusted pea protein

Solubility experiments were carried out at three conditions. First of all, solubility of the untreated samples was measured after pH adjustment to pH 6.0, 6.5, 7.0, 7.5 and 8.0 to characterise the individual influence of pH. In a subsequent step the pre-treated, lyophilised samples were re-dispersed at the pH value of their respective pre-treatment to characterise the additional impact of heating and homogenisation under those pH conditions. Last but not least solubility of the lyophilised samples re-dispersed at pH 8.0 was measured to differentiate irreversible loss of solubility from reversible loss and to simulate conditions at the beginning of fermentation.

Solubility of the untreated protein showed a significant pH dependency (table 2). Solubility decreased with decreasing pH and correlated with the ζ-potential (R=-0,939, table 3). Similar behaviour has been extensively described for various plant derived proteins e.g. (Barac et al., 2010) and can be ascribed to the formation of insoluble protein aggregates due to decrease in electrostatic repulsion with decreasing pH value. In a second step, the solubility of pre-treated, lyophilised samples at the pH-value of their respective pre-treatment was measured. Compared to the untreated protein at respective pH values, a further significant decrease of protein solubility (table 2) was found, indicating an additional influence of the pre-treatment process on protein solubility. Similar behaviour was previously reported for heating of soybeans (Nishinari, Fang, Guo, & Phillips, 2014).

Table 3: correlation matrix for results that showed significant differences in tables 2&4

	pH at heating [-]	Solubility (unheated) [%]	Solubility (heated,pH 8) [%]	G‘$_{end}$ [Pa]	G‘$_{24h}$ [Pa]	recovery [%]	loss of water [%]	ζ-potential [mV]
pH at heating [-]	1.000							
solubility$_{unheated}$ [%]	0.959***	1.000						
solubility$_{pH\ 8}$ [%]	0.885***	0.842***	1.000					
G‘end [Pa]	0.962***	0.971***	0.892***	1.000				
G‘24h [Pa]	0.932***	0.942***	0.910***	0.981***	1.000			
recovery [%]	0.911***	0.873***	0.771***	0.871***	0.860***	1.000		
loss of water [%]	-0.718***	-0.602**	-0.576**	-0.581**	-0.564**	-0.704***	1.000	
ζ-potential [mV]	-0.966***	-0.939***	-0.834***	-0,913***	-0,891***	-0,925***	0,746***	1.000
1^{rst} Peak area (SDS)	0.891***	0.851***	0.703***	0.797***	0.730***	0.852***	-0.582**	-0.884***

* α=0.1 ** α=0.05 *** α=0.01

Finally, from solubility experiments with lyophilised samples readjusted to simulate the starting pH of fermentation (pH 8) we obtained the following information. First of all, increasing the pH value increased the solubility compared to the values measured at the pH of pre-treatment and secondly, we found a decrease of solubility compared to the untreated sample at pH 8. The former can be ascribed to the presence of some pH reversible aggregates, that dissolve owing to the increased electrostatic repulsion upon increasing the pH. At the same time, the latter indicates an increase of insoluble aggregates caused by irreversible protein denaturation during the pre-treatment. This increase of insoluble aggregates was most pronounced in samples pre-treated at pH 6.0 and led to overall solubilities between 37.6 ±1.1% (pre-treatment at pH 6.0) and 57.2 ± 4.0% (pre-treatment at pH 8.0, table 2) with a correlation coefficient of R=0.885 (table 3). This indicates a shift in the proportions of soluble and insoluble fractions caused by the pH-value during pre-treatment. Higher protein solubility can be ascribed to a higher number of soluble aggregates and vice versa. More specific this means, that samples pre-treated at lower pH values contain fewer soluble and more insoluble aggregates than samples pre-treated at higher pH values. Since soluble aggregates are a prerequisite for gelation while insoluble

aggregates may act as inactive fillers (Britten & Giroux, 2001), the differently pre-treated samples are expected to exhibit differences in gelation behaviour.

Molecular weight distribution

SDS-PAGE is most suitable to investigate individual protein sub-fractions involved in aggregation since samples lose their quaternary structure and any non-covalent protein-protein interactions during sample preparation. Moreover, if SDS-PAGE is performed under reducing and non-reducing conditions, insights in the presence and constitution of disulphide bound aggregates can be gained. However, SDS-PAGE does not distinguish between soluble and insoluble aggregates. To this purpose SEC can be used to investigate the undenatured protein molecules and the formation of soluble aggregates. Consequently, applying both methods leads to a more detailed understanding of the aggregation behaviour of pea protein upon pre-treatment under different pH conditions and the protein fractions involved. For both types of investigation, the lyophilised samples were re-dispersed at the starting pH of fermentation (pH 8.0).

SDS-PAGE under reducing and non-reducing conditions (fig 2a) shows all bands typically expected in pea protein. In more detail, the major pea protein fractions are convicilin at ~70 kDa (Crévieu et al., 1997; Croy, Gatehouse, Tyler, & Boulter, 1980; Swanson, 1990), legumin at ~60 kDa (Croy, Gatehouse, Evans, & Boulter, 1980) and vicilin at ~50 kDa (Gatehouse, Croy, Morton, Tyler, & Boulter, 1981; Gatehouse, Lycett, Croy, & Boulter, 1982; Gatehouse, Lycett, Delauney, Croy, & Boulter, 1983). Moreover, legumin consists of an acidic α-chain (MW~38-40 kDa) and a basic β-chain (MW~20 kDa) (Croy, Derbyshire, Krishna, & Boulter, 1979; Croy, Gatehouse, Evans, et al., 1980), that are connected via a disulphide-bond and appear as separate bands on SDS-PAGE under reducing conditions. Vicilin on the other hand is prone to posttranslational autolysis which leads to various subunits of lower molecular weights (Dziuba, Szerszunowicz, Nalecz, & Dziuba, 2014; Gatehouse et al., 1982).

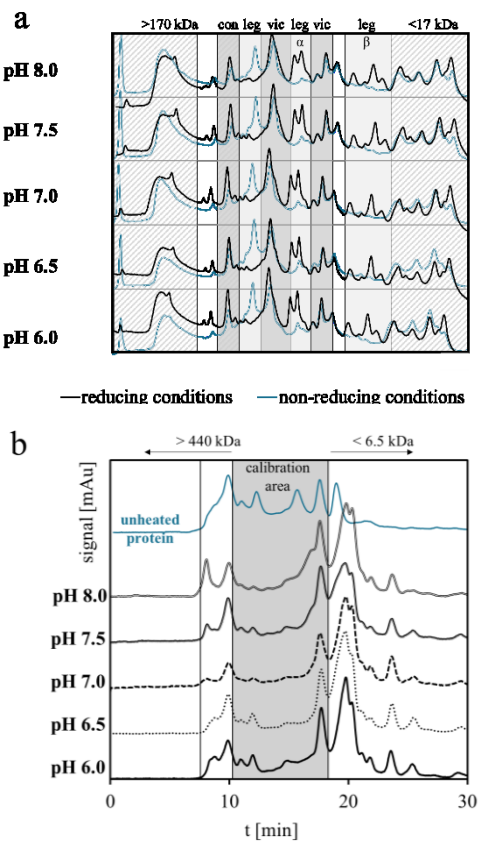

Fig 2 SDS-PAGE under reducing and non-reducing conditions (a) and SEC (b) of pea protein heated at pH 6 to 8.

Generally, fig 2a shows similar molecular weight profiles for all samples, independent of pH value during pre-treatment. Besides the bands regularly associated with pea protein, all samples contain two

fractions of protein > 170 kDa. Out of these, the fraction with lower molecular weight appears to remain unaffected by the pH value during pre-treatment and shows no relevant differences between reducing and non-reducing conditions. However, upon repetition of the experiment for a random sample with increased SDS-content in the sample buffer (results not shown) this fraction was decreased under reducing conditions, indicating aggregates held together by a mixture of disulphide bonds and strong, non-covalent interactions. The fraction with higher molecular weight only occurs as a prominent peak under non-reducing conditions and corresponds to fractions of the sample that did not migrate into the gel at these conditions. Since this peak is not present under reducing conditions, the previously retained aggregates must have been formed via disulphide bonds. Disulphide bonds can stabilise both, soluble and insoluble aggregates (table 1). Taking the results from solubility experiments (higher solubility at higher pH during pre-treatment) into account, the larger amount of retained fraction at higher pH during pre-treatment indicates an increased contribution of soluble disulphide bound aggregates.

Considering the aggregation behaviour known for soy where the 7S αα' (corresponding to pea convicilin) fraction forms soluble, disulphide bound aggregates with itself or the acidic 11S (corresponding to the legumin-α subunit) fractions (Yamagishi et al., 1983) (table 1) these soluble aggregates may be constituted from the corresponding pea protein fractions convicilin and legumin α. However, if legumin α subunits were involved, leftover legumin-β subunits (~20 kDa) should appear under non-reducing conditions. As this is not the case, we propose soluble disulphide bound aggregates to only consist of the convicilin fraction. Moreover, given the small differences in convicilin peak heights under reducing and non-reducing conditions, this type of aggregates is unlikely to be exclusively responsible for the retained, disulphide bound fractions. We therefore propose a mixture of soluble disulphide bound convicilin aggregates and various insoluble disulphide bound aggregates consisting of legumin and convicilin (Yamagishi et al., 1983) (table 1).

In SEC (fig 2b, blue line), the untreated pea protein included various fractions within the calibration area while results from pre-treated samples only showed very small fractions and fractions larger than 440 kDa. This indicates heat induced aggregation of legumin (~360 kDa (Croy et al., 1979)) vicilin (~150 kDa (Gatehouse et al., 1981)) and convicilin (280 kDa (Croy, Gatehouse, Tyler, et al., 1980)). Owing to the preliminary filtration step in the method, aggregates detected in SEC can be considered soluble and are therefore likely to consist of various combinations of vicilin, convicilin and convicilin plus legumin β (table 1). Fig 2b shows a decrease in these soluble aggregates with decreasing pH value during pre-treatment as indicated by the decrease in peak size of the peak at ~8 minutes, again supporting the conclusions drawn from protein solubility experiments and SDS-PAGE.

In summary, the combined results from protein solubility experiments, SDS-PAGE and SEC show a decrease in the number of disulphide-stabilised and soluble aggregates with decreasing pH during pre-treatment. Insoluble aggregates that may be stabilised via other types of interactions (especially hydrophobic ones) cannot be determined with either method due to sample preparation.

Gel characterisation

Kinetics of rheological parameters and pH value during fermentation

During fermentation, the pH value dropped from pH 8 to pH values around 4.8. Pre-treatment at different pH values did not significantly influence the kinetics or final pH value (table 4, fig S2a supplementary). In contrast, storage moduli (G') at the end of fermentation increased significantly with increasing pH values during pre-treatment (table 4 and fig S2b supplementary) and show a strong correlation (R = 0.842, table 3) to the protein solubility at the start of fermentation. Higher pH values during pre-treatment led to an increased number of soluble aggregates which are a prerequisite for network formation, while lower pH values led to an increased number of insoluble aggregates that may act as inactive fillers (Britten & Giroux, 2001). Larger numbers of soluble aggregates will lead to a higher degree of crosslinking and therefore to the formation of denser network structures with higher storage and loss moduli. In contrast, a larger proportion of insoluble aggregates reduces the number of soluble aggregates, which leads to a lower degree of crosslinking. Insoluble aggregates may additionally disturb the network formation by acting as inactive fillers. In combination, this leads to coarser network structures with lower moduli.

Table 4 pH, storage modulus G' and loss factor tan δ at the end of fermentation, G', recovery from thixotropy test, slope dlogG'/dlogω from frequency sweeps and loss of water after 24 hours of gel storage.

sample	pH_{end} [-]	G'_{end} [Pa]	tan δ_{end}	G'_{24h} [Pa]	recovery [%]	dlogG'/dlogω	loss of water [%]
pH 6.0	$4.75^{a}\pm 0.10$	$164^{a}\pm 84$	$0.167^{a}\pm 0.006$	$517^{a}\pm 164$	$14.1^{a}\pm 2.0$	$0.11^{a}\pm 0.01$	$4.8^{a}\pm 2.0$
pH 6.5	$4.77^{a}\pm 0.03$	$281^{a}\pm 80$	$0.158^{a}\pm 0.015$	$459^{a}\pm 63$	$21.3^{(\blacklozenge)}$	$0.14^{a}\pm 0.03$	$2.1^{(\blacklozenge)}$
pH 7.0	$4.79^{a}\pm 0.08$	$1623^{b}\pm 97$	$0.164^{a}\pm 0.005$	$2275^{a}\pm 238$	$28.7^{b}\pm 3.7$	$0.11^{a}\pm 0.02$	$0.9^{b}\pm 0.3$
pH 7.5	$4.82^{a}\pm 0.05$	$3665^{c}\pm 320$	$0.147^{a}\pm 0.006$	$4712^{b}\pm 678$	$32.0^{b}\pm 0.7$	$0.12^{a}\pm 0.00$	$1.0^{b}\pm 0.3$
pH 8.0	$4.77^{a}\pm 0.02$	$5488^{d}\pm 325$	$0.153^{a}\pm 0.003$	$7285^{c}\pm 1565$	$33.0^{b}\pm 2.6$	$0.11^{a}\pm 0.01$	$0.9^{b}\pm 0.8$

Different letters represent significant differences (α=0.05) as derived from ANOVA followed by Tukey post-Hoc test.

$^{(\blacklozenge)}$ value calculated from double determination due to equipment failure. Data point was excluded from ANOVA and post-Hoc test.

The differences in absolute values of G' and G'' caused by different pre-treatments did not affect the ratio between elastic and viscous proportions. Loss factor tan δ was similar for all samples (table 4), indicating similar viscoelastic network-properties under linear viscoelastic conditions at all pre-treatment conditions. If the viscoelastic network properties of gels produced from the same raw material under the same gelation conditions are similar while the absolute value of storage and loss modulus G' and G'' varies, it is reasonable to assume a similar general gelation mechanism based on similar types of interactions, where the main difference between samples is the number of available soluble aggregates and resulting degrees of crosslinking.

Characterisation of pea protein gels after resting at 4 °C for 24 hours

This proposed gel structure with different degrees of crosslinking was further investigated by small and large amplitude rheology, loss of water and CLSM experiments.

Frequency sweeps are generally used as an indicator for time dependent deformation of samples. In this context, short time behaviour is reflected by higher frequencies, and long-term behaviour by lower frequencies. In our study – independent of pre-treatment conditions – all samples showed a similar, low slope of log G' over log ω (table 4 and fig S3 supplementary) for the investigated frequency range. This is typical for gels and dispersions (Mezger, 2006). Furthermore, the values of ~0.12 were of the same magnitude as in our previous work (Klost & Drusch, 2019; Klost et al., 2020) and are in line with values reported for milk yoghurts (Hassan, Ipsen, Janzen, & Qvist, 2003). At lower frequencies, the storage modulus additionally indicates the degree of crosslinking. The higher the modulus, the higher the degree of crosslinking and vice versa (Mezger, 2006). For our samples this implies an increase in the degree of crosslinking and network density with increasing pH value during pre-treatment. Moreover, differences in network density were also found in CLSM experiments (fig 3). In gels made from protein pre-treated at pH 6.0 mainly large protein fragments are apparent with only a coarse network-structure visible. With increasing pH values during protein pre-treatment, the corresponding gels become denser and the number of large particles decreases.

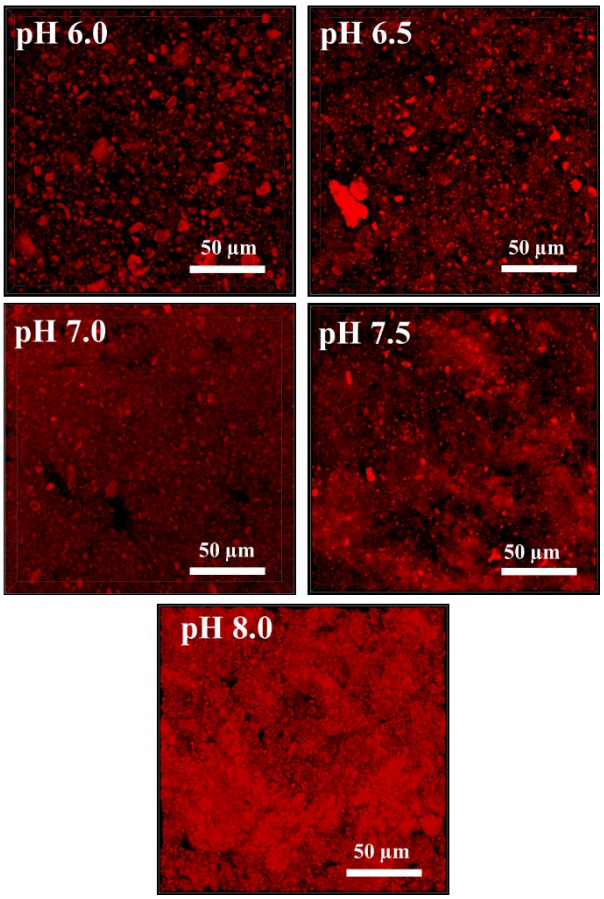

Fig 3 CLSM micrographs of fermentation induced pea protein gels made from pea protein slurry pre-treated at pH 6.0 to 8.0. pH values during pre-treatment are noted in the upper left-hand corner of the micrographs.

From thixotropy experiments we derive differences in the restructuring ability of the gels (table 4). The higher the pH during pre-treatment, the more pronounced was the structure recovery. Values ranged from 14.1 ± 2.0% at pH 6.0 to 33.0 ± 2.6% at pH 8.0 with pH 7.0 to pH 8.0 showing significantly higher recovery than samples pre-treated at pH 6.0. We ascribe these differences in structure recovery to the lower degree of crosslinking in samples pre-treated at lower pH values. In gels with lower degrees of crosslinking, the remaining network fragments are less likely to find a suitable counterpart for restructuring after intense shearing. Owing to their inactive filler properties, insoluble aggregates may additionally enhance this effect. In combination this leads to a decreased structure recovery. The results from thixotropy experiments correlate (R = -0.704, table 3) with the results from loss of water

experiments. Moreover, in loss of water experiments, samples made from protein pre-treated at pH 6.0 significantly differed from samples pre-treated at pH values ≥7.0. This increased loss of water after protein pre-treatment at low pH values is caused by larger pores in the coarser network structure of the corresponding gels.

Amplitude sweeps (fig 4) were performed to characterise the non-viscoelastic behaviour of the gels. Outside the linear viscoelastic regime, the rheological behaviour cannot exclusively be described by G' and G'' (fig 4a, top row) as higher harmonics become more relevant (Hyun et al., 2011). Appropriate additional means to interpret the transition from linear viscoelastic to non-linear viscoelastic behaviour as well as the non-linear viscoelastic behaviour itself are Lissajous plots (fig 4b), stress decomposition (fig 4c), dissipation ratio φ (fig 4a, middle row) and the calculation of the stiffening ratio (S-factor) (fig 4a, bottom row). Especially with regard to dissipation ratio φ and S-factor it needs to be kept in mind, that they describe the intracycle behaviour at a fixed intercycle strain amplitude γ_0, rather than the overall intercycle behaviour. Lissajous plots can be used to interpret the overall intercycle behaviour of gels as well as the intracycle deviation from linear viscoelastic behaviour by analysing their rotational behaviour and overall shapes. From stress decomposition a closer insight into the changes to elastic stress and more detailed knowledge on the intracycle stiffening/softening behaviour can be obtained. The calculation of S-factors reflects this intracycle behaviour onto the entire range of intercycle strain amplitudes γ_0 and the dissipation ratio φ can be applied to distinguish intracycle strain stiffening behaviour from effects caused by the transition from predominantly elastic to mainly plastic behaviour.

Results for all investigated samples in our study are shown in fig 4. Fig 4a shows the intercycle development of storage modulus G' and loss modulus G'' (top row), alongside the projection of intracycle parameters dissipation ratio φ and stiffening ratio (S-factor) on the entire range of investigated intercycle strain amplitudes γ_0 (middle and bottom row respectively). Fig 4b uses Lissajous plots to show the total stress τ over the intracycle strain γ for all samples at various intercycle strain amplitudes γ_0 and fig 4c shows the corresponding elastic stress τ' over the intracycle strain γ for all samples at various intercycle strain amplitudes γ_0.

Analogous to observations in all other rheological tests, results from amplitude sweeps showed similar curves of storage modulus G' and loss modulus G'' for all samples (fig 4a, top row). Between samples, these curves mainly differed in the absolute values of G' and G''. Linear viscoelastic regimes – calculated as intercycle strain amplitude γ_0 up to which G' deviated no more than 5% from the value at the lowest intercycle strain amplitude γ_0 – extended to $\gamma_0 \approx 1\%$ with no relevant influence of pH during pre-treatment.

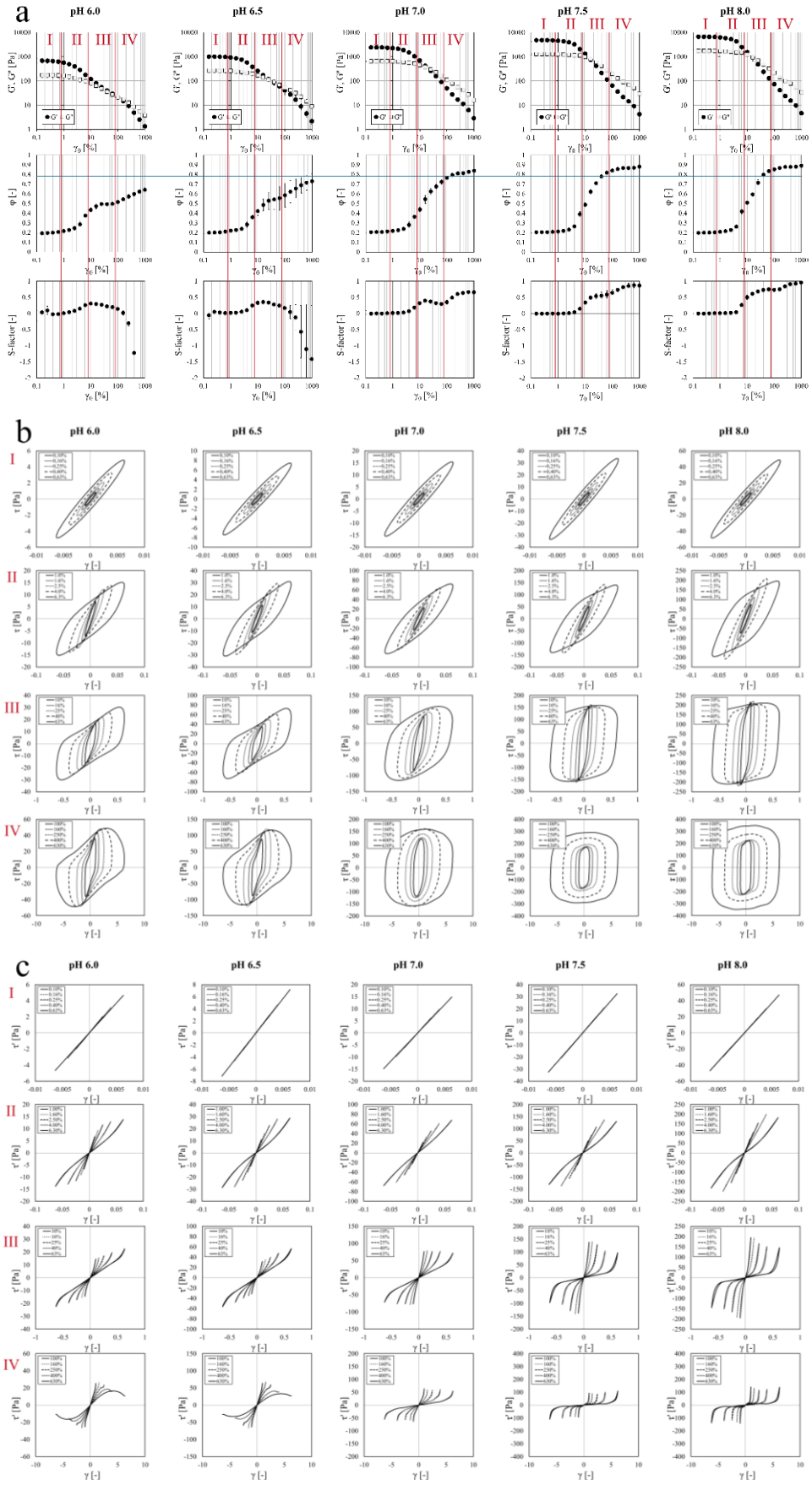

Fig 4 amplitude sweeps of fermentation induced pea protein gels made from pea protein pre-treated at pH 6.0 to 8.0 at intercycle strain amplitudes γ_0 between 0.1% and 1010% and a frequency of 1 s^{-1}. (a) top row: storage and loss modulus G' and G'' over, γ_0, (a) middle row: dissipation ratio φ over γ_0, (a) bottom row: stiffening ratio (S-factor) over γ_0, (b): elastic Lissajous plots, (c) elastic stress.

The extend of the linear viscoelastic regime is further supported by results from the dissipation ratio φ and S-factor, where constant values are remained up to intercycle strain amplitudes γ_0 between 1% and 2.5% (fig 4a, second and third row). Beyond the viscoelastic regime the overall intercycle rheological behaviour is strain softening. However, in order to take higher harmonics into account and to determine potential differences between samples it is worthwhile to also investigate the intracycle rheological behaviour by means of the parameters illustrated above.

At intercycle strain amplitudes γ_0 within the linear-viscoelastic regime ($\gamma_0 \leq 1\%$, marked "I" in fig 4a to c) elastic Lissajous plots (fig 4b I) have distinct elliptical shapes and the elastic stress τ' assumes the shape of a straight line (fig 4c I) as expected for linear viscoelastic behaviour. Moreover, no differences were observed between samples and the narrow shape of the Lissajous plots indicates predominantly elastic properties. This corresponds to the tan δ values, which are closer to zero than to one (table 4) and to dissipation ratios φ of approximately 0.2 (fig 4a I, middle row) that indicate predominantly elastic behaviour.

Lissajous plots and elastic stress τ' at intercycle strain amplitudes $1\% \leq \gamma_0 \leq 6.3\%$ (fig 4b and c II), begin to rotate clockwise with increasing intercycle strain amplitude γ_0, which indicates a gradual overall intercycle softening of the material (Ng, McKinley, & Ewoldt, 2011) and reflects the overall behaviour seen in fig 4a, top row. This behaviour is likely to be caused by alignment of network segments within the flow field or loss of network junctions that – similar to the effects observed in thixotropy tests – may lead to network segments which are unable to rejoin the network (Hyun et al., 2011). Moreover, in this range of intercycle strain amplitude γ_0 the shape of the Lissajous plots begins to get distorted from the elliptical shape, and elastic stress τ' starts to deviate from a straight line showing a clear impact of higher harmonics. However, depending on the pH value during pre-treatment, the distortion to the Lissajous plots is of different character and magnitude. If samples were pre-treated at pH 6.0 or pH 6.5, the corresponding elastic plots (fig 4d, II) begin to rotate and distort from an elliptical shape sooner, but the distortion appears to be gradual and fairly uniform. With increasing pH value during pre-treatment, rotation starts at higher amplitudes, and – especially for samples pre-treated at pH 7.5 and pH 8.0 – the distortion from elliptical shape starts more sudden ($\gamma_0 = 6.3\%$) and leads to more pronounced changes in shape. Lissajous plots from samples pre-treated at pH 7.0 show intermediate rotation and deformation behaviour. In addition, the shapes of the Lissajous plots are widening thus increasing the enclosed area indicating an increasingly dissipative response (Ng et al., 2011). This effect is further quantified in the dissipation ratio φ (fig 4a II second row) which starts to become dependent of the intercycle strain amplitude γ_0 and begins to increase, thus indicating a beginning shift from predominantly elastic behaviour towards an increasing contribution of plastic properties (Ewoldt et al., 2010). The deviation in the shape of Lissajous plots and the increase in dissipation ratio φ are accompanied by the transition of elastic stress τ' curves from a straight line towards an inversed sigmoidal shape. The decreased slope at low intracycle strain γ indicates a beginning reduction of size and volume fraction of rigid clusters

(Park et al., 2015) and supports the beginning shift from elastic to plastic properties, while the increasing slope at higher intracycle strain γ reflects the stretching of remaining clusters that cause intracycle stiffening (Park et al., 2015). This is reflected in the increase of the S-factor (fig 4a II, third row) which – in this range of intercycle stain amplitudes γ_0 is likely to be related to intracycle strain stiffening since the dissipation ratio φ is still well within the elastic range and the network structures only just began to be disrupted.

At intercycle strain γ_0 yet another order of magnitude higher ($10\% \leq \gamma_0 \leq 63\%$, fig 4b and c III) all shapes are distorted and show clear differences between samples. While Lissajous plots of samples pre-treated at pH 6.0 or pH 6.5 assume slightly bone shaped profiles, pre-treatment at pH 8.0 leads to Lissajous plots that are nearly rectangular shaped which implies an approximation towards perfect plastic behaviour (fig 4b and c III) (Ewoldt et al., 2010). Samples pre-treated at pH-values in between, show in-between distortions. In this range of intercycle strain amplitude γ_0 the clockwise rotation also proceeds, as visible in Lissajous plots, and – more distinctly – in the elastic stress (fig 4b III). Consequently, the slopes at small intracycle strain γ decrease further, indicating a continued intercycle strain softening behaviour owing to further reduction of rigid clusters. Nevertheless, at large intracycle strain the slope of the elastic stress still increases apparently indicating some remaining intracycle strain stiffening properties and therefore some residual elastic properties resulting in continuously positive S-factors in fig 4a III (third row). Despite overall similarities of the elastic stress curves, differences between samples become apparent in the considered range of intercycle strain γ_0. While samples pre-treated at pH 6.0 and pH 6.5 showed more moderate rotation and a less pronounced inversed sigmoidal shape, increased pH values during pre-treatment led to an almost horizontal slope at low intracycle strain γ which indicates an almost complete loss of rigid structures. These observations are reflected in the development of the dissipation ratio φ (fig 4a III, second row). While samples pre-treated at pH 6.0 and pH 6.5 only reach values in the range of $\varphi \approx 0.5$ in the discussed range of intracycle strain amplitudes γ_0 ($10\% \leq \gamma_0 \leq 63$) pre-treatment at pH 7.5 or pH 8.0 leads to $\varphi > \pi/4$ and therefore – in agreement with the vast loss of rigid structures deduced from elastic stress τ' and the shape of the Lissajous plots – the intracycle behaviour becomes predominantly plastic for these samples.

At the highest intercycle strain amplitudes γ_0 distortion of the Lissajous plots proceeds even further (fig 4b IV). In case of samples pre-treated at pH 6.0 and pH 6.5, the increase in dissipated energy as indicated by the increase of the enclosed area in Lissajous plots (fig 4b IV) is accompanied by a transition from intracycle strain stiffening to intracycle strain softening behaviour as derived from the shift of elastic stress τ' curves from inversed sigmoidal to sigmoidal shape at the highest intercycle strains γ_0. This shift is accompanied by a decrease of the S-factor below 0 and a second increase in the curves of the dissipation ratio φ. Despite the increase in dissipation ratio φ to final values of 0.64 ± 0.01 (pre-treatment at pH 6.0) and 0.73 ± 0.07 (pre-treatment at pH 6.5), these samples maintain a relevant proportion of elastic behaviour within the investigated deformation range, since final values of the

dissipation ratio φ remain below π/4 and the S-factors become negative. In contrast, for samples pre-treated at pH 7.0 to pH 8.0 the shapes approach rectangles with slightly rounded tops and bottoms which are similar to those described by (Ewoldt et al., 2010) for predominantly plastic systems. The shift to predominantly plastic behaviour is further reflected in the dissipation ratio φ that reaches final values of 0.84 ± 0.01, 0.88 ± 0.00 and 0.89 ± 0.00 for samples pre-treated at pH 7.0, pH 7.5 and pH 8.0 respectively and S-factors that increase further and approach final values of 0.66 ± 0.06, 0.87 ± 0.09 and 0.96 ± 0.03 respectively. Since positive S-factors generally indicate strain stiffening behaviour but may also indicate a transition from elastic to plastic behaviour as explained in the materials and methods section above, a closer investigation of the obtained S-factors is necessary. The curves of the S-factor (fig 4a, bottom row) show an indentation at the beginning of the considered amplitude range ($100\% \leq \gamma_0 \leq 630\%$, section IV) followed by a second increase. This indentation is most pronounced upon pre-treatment at pH 7.0 and decreases with increasing pH during pre-treatment. While it is reasonable to assume that in analogy to the curves of samples pre-treated at pH 6.0 and pH 6.5 the initial increase in these curves can be related to intracycle strain stiffening effects, this second increase must not necessarily be an indicator of continuing intracycle strain stiffening behaviour at the highest intercycle strain amplitudes γ_0. In fact, this would be very unlikely based on the presented results for elastic stress at the corresponding intercycle strain amplitudes γ_0 but can rather be explained by the fact, that in this case the tangent modulus at minimum intracycle strain γ (G_M) becomes negligible and the S-factor consequently diverges towards one as explained in the materials and methods section above for plastic behaviour (Ewoldt et al., 2010). Overall, these samples lost the majority of elastic properties while samples pre-treated at pH 6.0 and pH 6.5 retained a higher proportion of elastic properties. This leads to the conclusion, that coarser network structures are less prone to a complete transition towards plastic properties under the applied oscillatory strain conditions owing to an increased structural flexibility.

The underlying effects and differences between rheological behaviour of the samples outside the linear viscoelastic regime can best be related to their differences in network densities. In summary, all samples show intercycle strain softening, as derived from the clockwise rotation of the Lissajous plots (Ng et al., 2011) and elastic stress curves. For samples pre-treated at pH 6.0 and pH 6.5, the rotation starts sooner, indicating a higher flexibility of coarser networks to follow deformation, as a more flexible network is more likely to orient in the flow field. Additionally, the higher flexibility leads to a more gradual decrease in bond numbers and is reflected in transition from intracycle strain stiffening towards intracycle strain softening at higher intercycle strain γ_0. Denser gels (i.e. samples pre-treated at pH 7.0 to 8.0) are able to resist intercycle strain softening slightly longer, but – owing to their denser structures – have a higher degree of crosslinking and are therefore more prone to small microcracks (Faber et al., 2017) and decreasing bond numbers (Hsiao et al., 2012; Park & Ahn, 2013; Park et al., 2015) in the gel network. This in turn leads to the gradual disintegration of the gel and the transition from predominantly elastic properties to mainly plastic behaviour.

CONCLUSIONS

In summary our results show, that different pH values during pre-treatment of pea protein lead to different ratios between soluble and insoluble protein aggregates in the protein slurry before fermentation. These different ratios in turn are the determining factor, when it comes to the degree of crosslinking during gelation and the content of inactive fillers, that may disrupt the gel network structure and thus directly influence the rheological properties. It was found, that all gels showed frequency dependencies similar to milk yoghurts. However, storage and loss moduli were at significantly different magnitudes if pre-treatment was carried out between pH 6.5 and pH 8.0, confirming different degrees of crosslinking. Furthermore, the ability to recover network structures after intense shearing decreased with decreasing pH values during pre-treatment. Large amplitude oscillatory shear rheology indicated an overall intercycle strain softening behaviour and further confirmed differences in network densities. While denser networks started to decompose into smaller clusters sooner and eventually changed from predominantly elastic to mainly plastic behaviour, coarser networks displayed a higher flexibility towards deformation. Adjusting the pH value during pre-treatment of pea protein prior to fermentation induced gelation is therefore a valid tool for the customisation of the texture properties of pea protein-based yoghurt alternatives. With this knowledge in mind – besides catering to consumers preferences concerning yoghurt alternatives – further opportunities for the development of a wide range of fermented pea protein products with different texture requirements such as bread spreads, confectionary fillings etc. open up.

Acknowledgements:

The authors gratefully acknowledge the assistance and expertise of L. Barthel for CLSM measurements and the skilful lab-work of C. Härter as well as the proofreading by M. Brückner-Gühmann.

Funding:

This work was supported by NutriAct – Competence Cluster Nutrition Research Berlin-Potsdam funded by the Federal Ministry of Education and Research (BMBF) (FKZ: 01EA1806C).

References

Banovic, M., Lähteenmäki, L., Arvola, A., Pennanen, K., Duta, D. E., Brückner-Gühmann, M., & Grunert, K. G. (2018). Foods with increased protein content: A qualitative study on European consumer preferences and perceptions. *Appetite*, *125*, 233–243. https://doi.org/10.1016/j.appet.2018.01.034

Barac, M., Cabrilo, S., Pesic, M., Stanojevic, S., Zilic, S., Macej, O., & Ristic, N. (2010). Profile and functional properties of seed proteins from six pea (Pisum sativum) genotypes. *International Journal of Molecular Sciences*, *11*(12), 4973–4990. https://doi.org/10.3390/ijms11124973

Britten, M., & Giroux, H. J. (2001). Acid-induced gelation of whey protein polymers: Effects of pH and calcium concentration during polymerization. *Food Hydrocolloids*, *15*(4–6), 609–617. https://doi.org/10.1016/S0268-005X(01)00049-2

Cairoli, S., Iametti, S., & Bonomi, F. (1994). Reversible and irreversible modifications of β-lactoglobulin upon exposure to heat. *Journal of Protein Chemistry*, *13*(3), 347–354. https://doi.org/10.1007/BF01901568

Cano-Sarmiento, C., Téllez-Medina, D. I., Viveros-Contreras, R., Cornejo-Mazón, M., Figueroa-Hernández, C. Y., García-Armenta, E., … Gutiérrez-López, G. F. (2018). Zeta Potential of Food Matrices. *Food Engineering Reviews*, *10*(3), 113–138. https://doi.org/10.1007/s12393-018-9176-z

Crévieu, I., Carré, B., Chagneau, A.-M., Quillien, L., Guéguen, J., & Bérot, S. (1997). Identification of Resistant Pea (Pisum sativum L.) Proteins in the Digestive Tract of Chickens. *Journal of Agricultural and Food Chemistry*, *45*(4), 1295–1300. https://doi.org/10.1021/jf960806b

Croy, R., Derbyshire, E., Krishna, T., & Boulter, D. (1979). Legumin of pisum sativum and vicia faba. *The New Phytologist*, 29–35.

Croy, R., Gatehouse, J., Evans, I., & Boulter, D. (1980). Characterisation of the storage protein subunits synthesised in vitro by polyribosomes and RNA from developing pea (Pisum sativum L.) - I. Legumin. *Planta*, *148*(1), 49–56. https://doi.org/10.1007/BF00385441

Croy, R., Gatehouse, J., Tyler, M., & Boulter, D. (1980). The purification and characterization of a third storage protein (convicilin) from the seeds of pea (Pisum sativum L.). *Biochemical Journal*, *191*(2), 509–516. https://doi.org/10.1042/bj1910509

Damodaran, S., & Kinsella, J. E. (1982). Effect of Conglycinin on the Thermal Aggregation of Glycinin. *Journal of Agricultural and Food Chemistry*, *30*(5), 812–817. https://doi.org/10.1021/jf00113a003

Dickinson, E. (2009). Hydrocolloids as emulsifiers and emulsion stabilizers. *Food Hydrocolloids*, *23*(6), 1473–1482. https://doi.org/10.1016/j.foodhyd.2008.08.005

Dziuba, J., Szerszunowicz, I., Nalecz, D., & Dziuba, M. (2014). Proteomic Analysis of Albumin and Globulin Fractions of Pea (Pisum Sativum L .) Seeds *. *Acta Scientarium Polonorum*, *13*, 181–190.

Ewoldt, R. H., Hosoi, A. E., & McKinley, G. H. (2008). New measures for characterizing nonlinear viscoelasticity in large amplitude oscillatory shear. *Journal of Rheology*, *52*(6), 1427–1458. https://doi.org/10.1122/1.2970095

Ewoldt, R. H., Winter, P., Maxey, J., & McKinley, G. H. (2010). Large amplitude oscillatory shear of pseudoplastic and elastoviscoplastic materials. *Rheologica Acta*, *49*(2), 191–212. https://doi.org/10.1007/s00397-009-0403-7

Faber, T. J., Van Breemen, L. C. A., & McKinley, G. H. (2017). From firm to fluid – Structure-texture relations of filled gels probed under Large Amplitude Oscillatory Shear. *Journal of Food Engineering*, *210*, 1–18. https://doi.org/10.1016/j.jfoodeng.2017.03.028

Gatehouse, J., Croy, R., Morton, H., Tyler, M., & Boulter, D. (1981). Characterisation and Subunit Structures of the Vicilin Storage Proteins of Pea (Pisum sativum L.). *European Journal of Biochemistry*, *118*(3), 627–633. https://doi.org/10.1111/j.1432-1033.1981.tb05565.x

Gatehouse, J., Lycett, G., Croy, R., & Boulter, D. (1982). The post-translational proteolysis of the subunits of vicilin from pea (Pisum sativum L.). *Biochemical Journal*, *207*(3), 629–632. https://doi.org/10.1042/bj2070629

Gatehouse, J., Lycett, G., Delauney, A., Croy, R., & Boulter, D. (1983). Sequence specificity of the post- translational proteolytic cleavage of vicilin, a seed storage protein of pea (Pisum sativum L.). *Biochemical Journal*, *212*, 427–432.

German, B., Damodaran, S., & Kinsella, J. E. (1982). Thermal Dissociation and Association Behavior of Soy Proteins. *Journal of Agricultural and Food Chemistry*, *30*(5), 807–811. https://doi.org/10.1021/jf00113a002

Guzmán-González, M., Morais, F., Ramos, M., & Amigo, L. (1999). Influence of skimmed milk

concentrate replacement by dry dairy products in a low fat set-type yoghurt model system. I: Use of whey protein concentrates, milk protein concentrates and skimmed milk powder. *Journal of the Science of Food and Agriculture*, *79*(8), 1117–1122. https://doi.org/10.1002/(SICI)1097-0010(199906)79:8<1117::AID-JSFA335>3.3.CO;2-6

Hassan, A. N., Ipsen, R., Janzen, T., & Qvist, K. B. (2003). Microstructure and rheology of yogurt made with cultures differing only in their ability to produce exopolysaccharides. *Journal of Dairy Science*, *86*(5), 1632–1638. https://doi.org/10.3168/jds.S0022-0302(03)73748-5

Hsiao, L. C., Newman, R. S., Glotzer, S. C., & Solomon, M. J. (2012). Role of isostaticity and load-bearing microstructure in the elasticity of yielded colloidal gels. *Proceedings of the National Academy of Sciences of the United States of America*, *109*(40), 16029–16034. https://doi.org/10.1073/pnas.1206742109

Hyun, K., Wilhelm, M., Klein, C., Cho, K., Nam, J., Ahn, K., … McKinley, G. (2011). A review of nonlinear oscillatory shear tests: Analysis and application of large amplitude oscillatory shear (LAOS). *Progress in Polymer Science (Oxford)*, *36*(12), 1697–1753. https://doi.org/10.1016/j.progpolymsci.2011.02.002

Klemmer, K. J., Waldner, L., Stone, A., Low, N. H., & Nickerson, M. T. (2012). Complex coacervation of pea protein isolate and alginate polysaccharides. *Food Chemistry*, *130*(3), 710–715. https://doi.org/10.1016/j.foodchem.2011.07.114

Klost, M., & Drusch, S. (2019). Structure formation and rheological properties of pea protein-based gels. *Food Hydrocolloids*, *94*(September), 622–630. https://doi.org/10.1016/j.foodhyd.2019.03.030

Klost, M., Giménez-Ribes, G., & Drusch, S. (2020). Enzymatic hydrolysis of pea protein: Interactions and protein fractions involved in fermentation induced gels and their influence on rheological properties. *Food Hydrocolloids*, *105*, 105793. https://doi.org/10.1016/j.foodhyd.2020.105793

Krajcovicova-Kudlackova, M., Babinska, K., & Valachovicova, M. (2005). Health benefits and risks of plant proteins. *Bratislavské Lekárske Listy*, *106*(6–7), 231–234.

Mermet-Guyennet, M. R. B., Gianfelice de Castro, J., Habibi, M., Martzel, N., Denn, M. M., & Bonn, D. (2015). LAOS: The strain softening/strain hardening paradox. *Journal of Rheology*, *59*(1), 21–32. https://doi.org/10.1122/1.4902000

Mezger, T. (2006). *Das Rheologie Handbuch* (2nd ed.). Hannover: Vincentz Network GmbH & Co. KG.

Ng, T. S. K., McKinley, G. H., & Ewoldt, R. H. (2011). Large amplitude oscillatory shear flow of gluten dough: A model power-law gel. *Journal of Rheology*, *55*(3), 627–654.

https://doi.org/10.1122/1.3570340

Nishinari, K., Fang, Y., Guo, S., & Phillips, G. O. (2014). Soy proteins: A review on composition, aggregation and emulsification. *Food Hydrocolloids*, *39*, 301–318. https://doi.org/10.1016/j.foodhyd.2014.01.013

Park, J. D., & Ahn, K. H. (2013). Structural evolution of colloidal gels at intermediate volume fraction under start-up of shear flow. *Soft Matter*, *9*(48), 11650–11662. https://doi.org/10.1039/c3sm52090k

Park, J. D., Ahn, K. H., & Lee, S. J. (2015). Structural change and dynamics of colloidal gels under oscillatory shear flow. *Soft Matter*, *11*(48), 9262–9272. https://doi.org/10.1039/c5sm01651g

Petruccelli, S., & Añón, M. C. (1995). Thermal Aggregation of Soy Protein Isolates. *Journal of Agricultural and Food Chemistry*, *43*(12), 3035–3041. https://doi.org/10.1021/jf00060a009

Piorkowski, D. T., & McClements, D. J. (2014). Beverage emulsions: Recent developments in formulation, production, and applications. *Food Hydrocolloids*, *42*, 5–41. https://doi.org/10.1016/j.foodhyd.2013.07.009

Ringgenberg, E., Alexander, M., & Corredig, M. (2013). Effect of concentration and incubation temperature on the acid induced aggregation of soymilk. *Food Hydrocolloids*, *30*(1), 463–469. https://doi.org/10.1016/j.foodhyd.2012.05.011

Schneider, C. A., Rasband, W. S., & Eliceiri, K. W. (2012). NIH Image to ImageJ: 25 years of image analysis. *Nature America*, *9*, 671–675.

Swanson, B. G. (1990). Pea and Lentil Protein Extraction and Functionality. *Journal of the American Oil Chemists' Society*, *67*(5), 276–280.

WHO. (2013). Draft action plan for the prevention and control of noncommunicable diseases 2013 – 2020. *Report by the Secretariat*, (April), 1–50.

Yamagishi, T., Miyakawa, A., Noda, N., & Yamauchi, F. (1983). Isolation and Electrophoretic Analysis of Heat-induced Products of Mixed Soybean 7S and 11S Globulins. *Agricultural and Biological Chemistry*, *47*(6), 1229–1237. https://doi.org/10.1271/bbb1961.47.1229

SUPPLEMENTARY

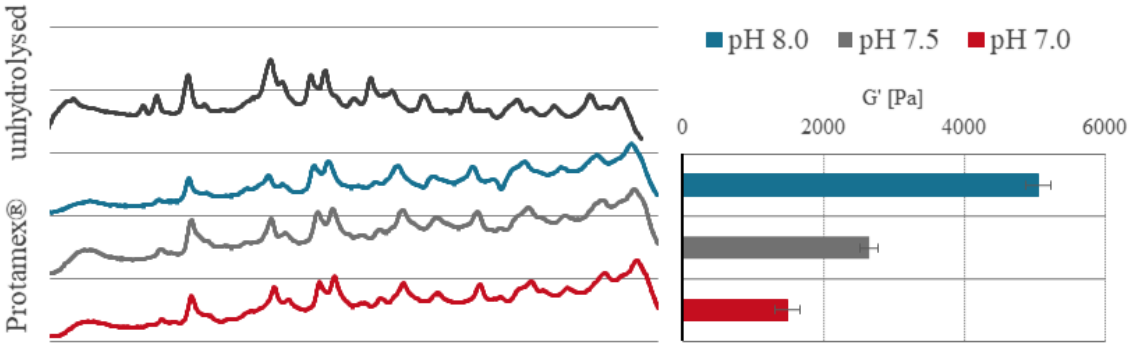

Fig S 1 Molecular weight profile of pea protein (black) and pea protein hydrolysed with Protamex® under different pH conditions (blue: pH 8.0, grey: pH 7.5, red: pH 7.0) and storage moduli G' of the corresponding fermentation induced gels.

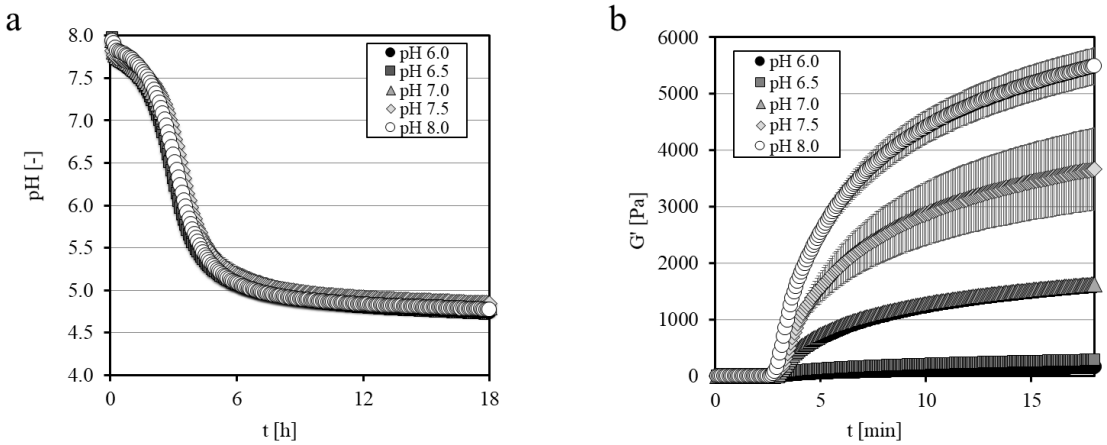

Fig S2 pH-drop (a) and increase of G' (b) during fermentation of pea protein preheated at different pH-values.

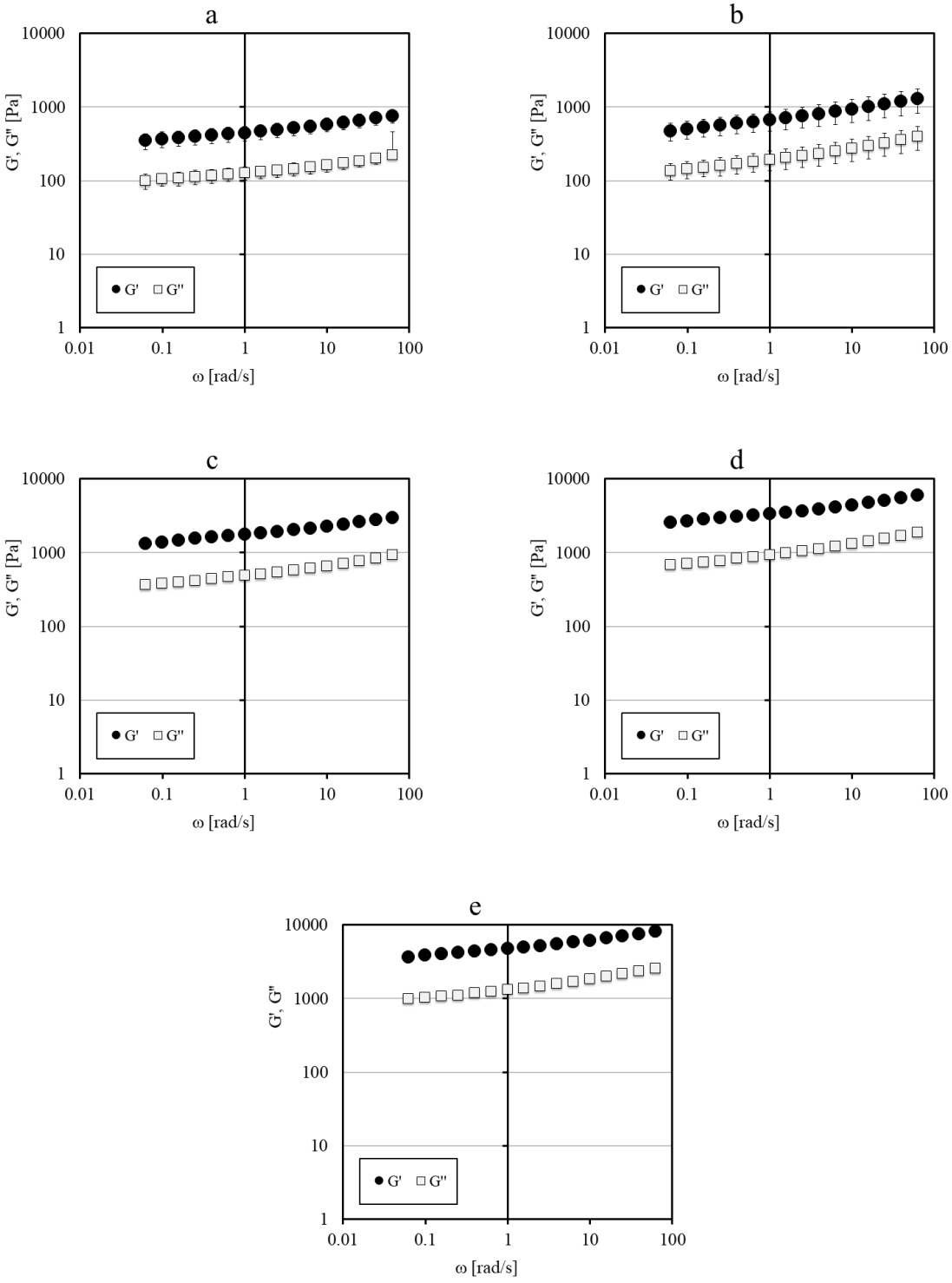

Fig S3 G' and G'' in frequency sweeps pH 6.0 (a), pH 6.5 (b), pH 7.0 (c), pH 7.5 (d), pH 8.0 (e)